

A Practical Ultrasonic Inspection Method for Detecting and Characterising Defects Found Within Composite Repairs

Co-Authored by: J.Downing BEng (Hons) MSc DipIC CEng MIMechE and A.Hook BSc (Hons) AMRINA

Synopsis

Two steel substrate test panels were developed to represent common plate thicknesses found on naval vessels and scanned using the Babcock developed ultrasonic technique. One sample comprised of a series of slotted surface breaking flaws of varying widths and through thicknesses to represent fracturing/cracking. The inspection method detected simulated cracking to a depth of 2mm and 0.5mm in width. The second sample included numerous loss of wall thickness areas of varying diameters and through thicknesses, with the smallest detectable loss of wall thickness being 0.1mm at a 15mm diameter. After proving confidence in detection, there was a need to characterise flaws to provide support and ascertain a repair action. Samples were produced that were subjected to either impact or heat exposure to induce realistic representative damage. The practical ultrasonic method was successfully used to independently characterise between the samples, with induced de-laminations caused by blisters, and multi layered matrix cracking caused by varying levels of projectile impacts, due to their unique morphology.

Keywords: Phased Array Ultrasonic Testing, Composite Repair, Fibre Volume Fraction, Void Content, Composite Flaw Characterisation, Glass Fibre Reinforced Plastic, Carbon Fibre Reinforced Plastic.

1. Introduction: Moving away from weld and insert repairs

The vast majority of primary and secondary naval metallic structural repairs are completed through the use of welding and inserts, which is time consuming and costly when compared to the opportunities of using composite repairs. However, composite repairs on ship primary and secondary structure are currently restricted as there is no accepted method of detecting defects in metal substrates that are bonded to composite materials. Proving that a range of defects can be detected in this type of structure therefore opens up an expansive business area.

Hence, the challenge is to ensure confidence in a permanent composite repair solution using current simulation techniques to monitor repaired structures through life, e.g. bond layer performance, impact and heat response, corrosion/loss of wall thickness and substrate crack growth rates, with a view to achieving improvements in:

- Confirming laminate integrity.
- Confirming steel/composite bond integrity.
- Measuring substrate thickness through laminate, i.e. recording wastage rates.
- Identifying substrate flaws through the laminate, i.e. monitoring crack growth.

Composite strengthening is attractive on ship structures because:

- Welding and work-in-way is significantly reduced, e.g. strengthening a corroded deck above a Control Room without disturbing the deckhead below reduces workload significantly and provides considerable cost and programme benefits.
- Enhancing fatigue strength with composites does not introduce new residual stresses through welding, or weakening in high strength steels around the weld heat affected zones, hence the surrounding structure retains more of its as built properties.

The principal project aim was to assess a practical ultrasonic inspection method for detecting and characterising individual in-service flaws found within the following composite repairs:

- 10mm Steel substrate plate bonded to 10mm Carbon Fibre Reinforced Plastic (CFRP):
 - Far-surface and sub-surface flaws within steel:
 - Loss of wall thickness (corrosion/pitting).
 - Fatigue cracking perpendicular to the beam.
 - De-bonding between the metallic and composite material interfaces.
- 16 Glass Fibre Reinforced Plastic (GFRP) Vinyl Ester test samples, 10mm thick:
 - 10 samples subjected to a range of $\approx 15\text{-}74\text{J}$ impact tests of projectile kinetic energy producing multi-layered matrix cracking/micro-de-laminations.
 - 6 samples exposed to an acute high temperature source for a period of 2 to 3.5 minutes producing de-laminations.

There is a need to be able to characterise flaws arising in GFRP composite naval assets to provide confidence to Design Authorities so they are able to confidently ascertain a go/no-go repair.

2. Phased Array Ultrasonic Testing of Composites

Ultrasonic Testing (UT) inspection is one of the primary NDT methods/technologies in use today for in-service examination of composite structures, especially regarding the capability for the detection, sizing and depth estimation of flaws. However, there is currently no accepted method of detecting defects in metal substrates that are bonded to composite materials.

Phased Array Ultrasonic Testing (PAUT) technology differs from traditional UT in that the energy can be controlled more finitely to focus and steer the beam, providing the best capabilities for in-service inspection. Ultrasonic waves from a single crystal probe are emitted as a single source energy that radiates out in to a medium, which is modified electronically by pulsing each individual crystal in the array to generate small waves that interact with each other causing a predetermined wave front. This interaction can be exploited to obtain beam focussing and steering. Each element is excited in a sequential time separation which is known as phasing (also applied to the returning signal), hence the term Phased Array (PA).

Linear array PA probes were used based on theoretical and practical experience, combined with equipment availability and compatibility. The data, information and observations were gathered using the Olympus MX2 unit, and analysed using the TomoView[®] and OmniPC[®] software packages.

Once the scan is complete, data is exported to TomoView[®] analysis software, which allows production of four image types (A-, B-, C- and D-Scans) that can be manipulated into a 3D image (Figure 1) or analysed in slices. Data can be permanently stored, allowing comparison against the historical state of the structure.

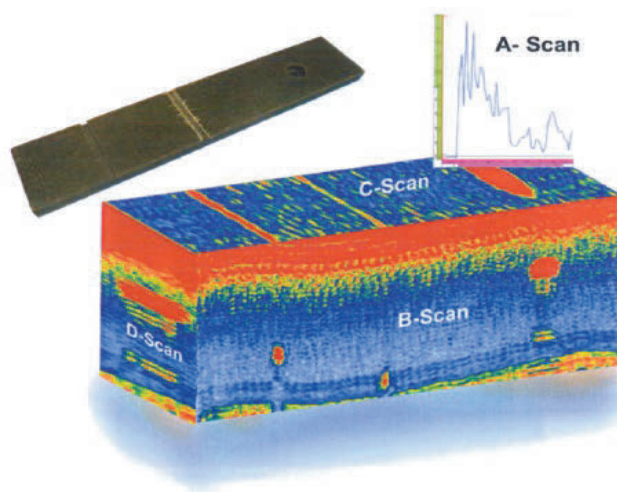


Figure 1 – PA Analysis Software of CFRP Calibration Piece

3. PAUT to Detect Flaws in Composite to Metallic Bonded Substrates

PAUT inspection was used to investigate the test pieces, with the results correlated against the known flaw size and position in order to evaluate the accuracy, reliability and repeatability. The flaws were assessed against the minimum acceptance standards as detailed within Defence-Standards (Def-Stan) 02-729, 02-752 and 08-145. Hence, detection of the following synthetic flaws, with respect to their size and not morphology, validated this inspection technique, i.e. anything larger would require repair:

- 20mm diameter / 1mm thick.
- 10mm diameter / 0.25mm thick (representative of single ply thick voids and de-bonding).
- Corrosion and fatigue cracking (general pressure hull structure):
 - Any flaw less than or equal to 100mm in length.
 - Any flaw less than or equal to 50% of the plate thickness.
- Corrosion (primary structure):
 - General wastage less than or equal to 3% of plate thickness.

As no standard exists for the identification of fatigue cracking type flaws it was decided that the simulated flaws should be parallel with regards to the PAUT technique used for detection, i.e. cracking at a 0° angle with respect to the PA beam. This represents the most difficult to detect flaw as the PAUT technique primarily uses a 0° compressional beam that will identify the smallest plan surface area of the crack. If the crack is hit at an angle using shear waves (illustrated by Figure 2) it will provide a surface area greater than the 2.925mm and 1.535mm smallest detectable flaws as expressed by Equation [1], hence the potential to identify this flaw type would increase.

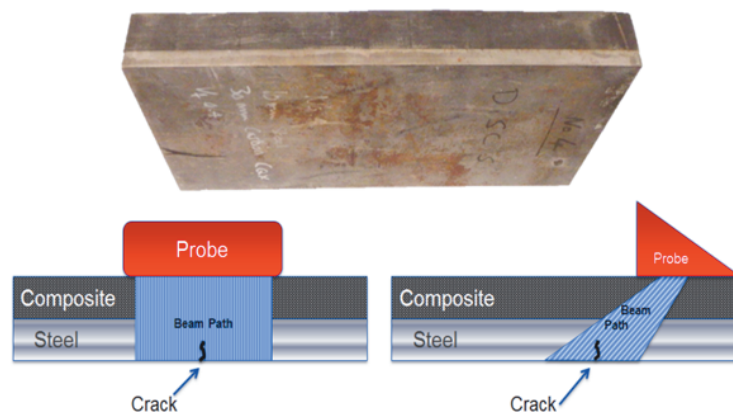


Figure 2 – Shear Waves to Detect Cracks

$$\text{Steel: } \frac{1}{2} \lambda = \left(\frac{V}{f} \right) \div 2 \rightarrow \frac{1}{2} \lambda = \left(\frac{5850}{1 \times 10^6} \right) \div 2 \rightarrow \frac{1}{2} \lambda = 0.002925\text{m} = 2.925\text{mm}$$

$$\text{Composite: } \frac{1}{2} \lambda = \left(\frac{V}{f} \right) \div 2 \rightarrow \frac{1}{2} \lambda = \left(\frac{3070}{1 \times 10^6} \right) \div 2 \rightarrow \frac{1}{2} \lambda = 0.001535\text{m} = 1.535\text{mm}$$

Equation 1 – Smallest Detectable Flaw

3.1. Method Validity

3.1.1. CFRP Test Pieces

Two 10mm thick steel test piece specimens were fabricated to conform to Def-Stan 02-729, with a range of flaws of a known type, size and position artificially manufactured to simulate:

- Steel substrate cracks – 9 spark eroded slotted flaws of varying widths and through thicknesses, perpendicular to the scanning interface (Figure 3 – Test Piece 1):
 - 2mm to 0.5mm wide.

- Recessed depths ranged from 2mm to 5mm, allowing inspection sensitivity to be measured from 20% to 50% of the 10mm steel plate thickness.
- De-bonding between the bonded CFRP to steel interface – 6 Polytetrafluoroethylene (PTFE) disk inserts of varying diameters, each 0.25mm thick (Figure 3 – Test Piece 1).
- Steel substrate loss of wall thickness – 35 milled circular flaws of varying diameters and recessed depths (Figure 4 – Piece 2):
 - Circular areas (30mm to 2.5mm diameter).
 - Recessed depths ranged from 0.1mm to 5mm, allowing inspection sensitivity to be measured from 1% to 50% of the 10mm steel plate thickness.

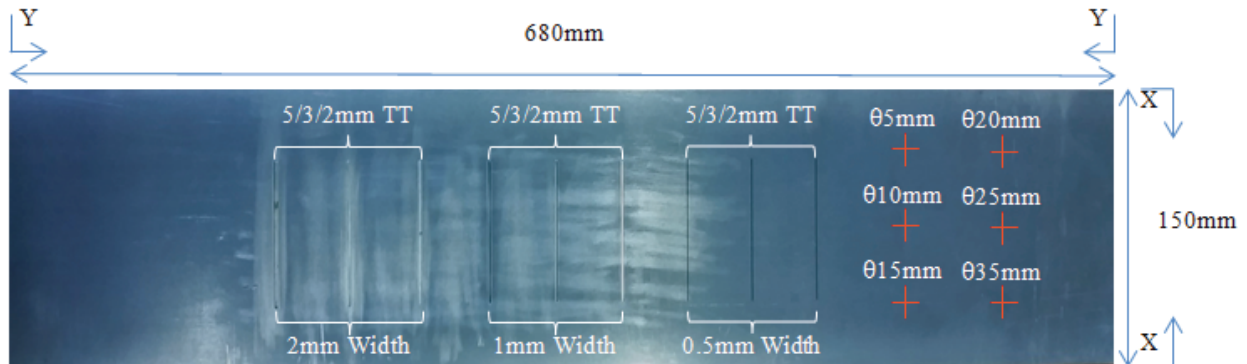


Figure 3 – Test Piece 1

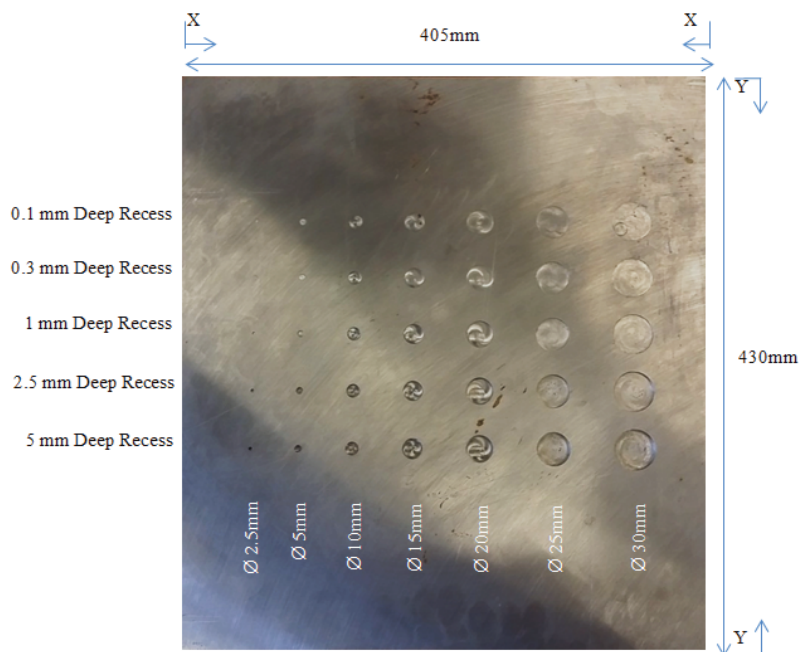


Figure 4 – Test Piece 2

The steel test pieces were laminated with 10mm of CFRP using two techniques for comparative assessment:

1. Laboratory based Resin Infusion under Flexible Tooling (RIFT) at the University of Plymouth.
2. In-service hand laminated and vacuum consolidated undertaken in Babcock's composite facility.

Hand laminating is a common composite repair method to return the material back to the desired strength and most notably to the same thickness as the parent metallic material. Typically, this method of using CFRP in place of steel results in strength and stiffness properties in excess of original build-specification (an accepted practice to maintain surface linearity and prevent de-bonding at interfaces). Repairs to pipes and other complex structure are bespoke as they are dependent on location, strength requirements and type/use.

Although preformed composite plates have been bonded in place in some applications, generally the geometry of a ship structure dictates that the composite is laminated in situ, i.e. conventional wet layup with vacuum consolidation. However, regardless of technique, good surface preparation of the substrate is critical, as is maintaining a good Quality Assurance record of the process to ensure the final laminate is of the correct quality and physical properties, e.g. sample pieces of the laminate made alongside the job for subsequent testing to confirm the design values of tensile strength and inter-laminar adhesion are achieved.

The same two following reinforcement types were used for both lamination techniques:

1. Carbon Fibre
 - a. Compromise between adding appropriate number of plies and the practicality of impregnating more layers, which promotes higher fibre volume (V_F) fractions and lower void content (V_V).
2. Glass Fibre
 - a. Prevents galvanic corrosion between the steel and carbon mating faces.
 - b. Superior wet out and drape compared to woven roving, with a small reduction in stability, hence more easily conforming to a surface and improving the bond.
 - c. Low areal weight promotes resin flow at the interface, improving the bond.

Two different types of epoxy based matrix were chosen for each lamination technique due to their incredible toughness and consistent bonding strength, high resistance to moisture absorption and ease of use:

1. Epoxy resin laminating system for RIFT.
2. Epoxy for resin vacuum infusion.

Laminate properties evaluation was completed for the test pieces with composite density, fibre resin fraction and void content determined by immersed mass comparison and resin burn-off testing (summarised in Table 1).

Test Piece	Composite ρ (Kg/m ³)	V_F (%)	V_R (%)	V_V (%)
Laboratory Test Piece 1 (Slotted)	1519.7	60.8	38.4	0.78
Laboratory Test Piece 2 (Circles)	1535.6	62.9	36.5	0.60
In-Service Test Piece 2 (Circles)	1438.2	57.9	35.9	6.26

Table 1 – Test Laminate Properties Summary

Each sample was examined using the developed PAUT method following the test steps below. Single plane A-, B-, C- and D-scan data was used to locate flaws, with further refinement available through B- and D-scan projection using gate selectors, which has the effect of reducing interference patterns from single plane flaws. The S-scan (sectorial-scan) display gives an inspection that sweeps through a range of angles, used for analysing beam steered data. The contrast/exposure of the palette was used to fine tune, post locating flaws, to accentuate their visual profile and enable more accurate sizing, operating on a similar principle of increasing or decreasing gain.

Test Method 1 – Olympus 0° PA Wheel Probe Roller Scanner (1MHz and 5MHz):

1. Test Pieces 1 and 2 to identify:
 - a. Loss of wall thickness, i.e. what is the smallest diameter and through thickness flaw that can be identified.
 - b. De-bonding between steel and composite.
 - c. Crack type flaws.
2. Single pass scanning in direction as shown in Figure 6 and Figure 7.

Test Method 2 – Olympus 0° PA Fixed Wedge and Probe:

1. Test Piece 1 to identify:
 - a. De-bonding between steel and composite, i.e. PTFE discs.
 - b. Crack type flaws.
2. Single pass scanning in direction as shown in Figure 7.
3. Combinations of 5mm, 10mm and 20mm offsets and 7°, 10°, 12.5° and 15° beam steered angles.
 - a. Multiple single crystal UT linear array probes used to generate multiple waves using differing delays, i.e. to enable beam ‘steering’ and improve sensitivity in the area of interest.

3.1.2. GFRP Test Pieces

In the absence of any up-to-date or applicable standards, an experimental based project was undertaken utilising the practical PAUT ultrasonic method, which can be used on in-service maintenance periods to distinguish between de-laminations caused by blisters, and multi-layered matrix cracking/micro-de-laminations caused by impacts.

16 GFRP Vinyl Ester test samples, 10mm thick, were manufactured under vacuum assisted resin infusion. 10 of the samples were subjected to impact testing with a range of $\approx 15\text{-}74\text{J}$ of projectile kinetic energy, and 6 samples exposed to an acute high temperature source for a period of 2 to 3.5 minutes.

The impact test was conducted with two hemispherical ended impact weights (5Kg and 10Kg) that were manufactured and individually dropped under a guided delivery system, with an incorporated anti-bounce mechanism, at varying heights. The aim of this test was to create varying levels of damage including matrix cracking and de-laminations.

The heat exposure test was conducted at a distance of 55mm from the surface at 30 second intervals with temperatures ranging from 250-400°C. The aim of this test was to produce surface blistering that subsequently causes de-laminations.

After the destructive testing was carried out, all test samples were subjected to advanced ultrasonic testing. The equipment used was a Phased Array immersion roller scanner connected to a Phased Array acquisition unit flaw detector. The ultrasonic scans were taken in strips of 45mm, coupled to the laminate surface using water.

All post processing of the NDT examinations was completed using TomoView[®] software with files converted and strips merged as necessary so the A-, B-, C- and D-scan of each sample could be viewed independently, slice-by-slice for scrutiny and characterisation. To confirm the flaw identified by PAUT and subsequently characterise it, a macro slice was made in each sample using a diamond coated blade, sliced down the vertical plane where the volumetric damage can be identified. This exposed the centre face of the damaged area that was viewed under an optical microscope and, where required, a Scanning Electron Microscope (SEM).

3.2. Results

3.2.1. CFRP Test Pieces

Table 2 highlights the minimum flaw detection results identified by PAUT for both test methods against the Def-Stan code compliance requirements.

Def-Stan	Compliance Requirements	Compliance Requirements Met	Minimum Flaw Detection Characteristics
02-729	De-bonding < 050mm	Yes	05mm (0.25mm PTFE Wall Thickness (WT))
02-752	De-bonding < 071.3mm	Yes	
08-145	Flaws $\leq 100\text{mm}$ in Length	Yes	Loss of WT: - L1.5: 0.3mm (2.98%) WT loss at 05mm (illustrated in Figure 8) - L1.7.2: 0.1mm (0.99%) WT loss at 015mm (illustrated in Figure 38) Cracking: - L2.2: 0.5mm Width at 2mm (20%) Through WT (illustrated in Figure 39 and Figure 40)
	Flaws $\leq 7.5\text{mm}$ in Through Wall Thickness	Yes	
	Flaws $\leq 50\%$ of the Plate Thickness	Yes	
	General Wastage $\leq 3\%$ Plate Thickness	Yes	
	Individual Flaw Wastage $\leq 5\%$ Plate Thickness	Yes	

Table 2 – Def-Stan Code Compliance

Additionally, the results identified the following clear distinction in flaw detection between the in-service and laboratory test pieces:

- In-service Test Pieces:
 - De-bonding flaws identified = 6 of 6 (100%).

- Cracks identified = 0 of 9 (0%).
- Loss of wall thickness flaws identified = 15 of 35 (42.86%).
- Minimum WT loss identified (against total steel plate thickness) = 9.94%.
- Laboratory Test Pieces:
 - De-bonding flaws identified = 6 of 6 (100%).
 - Cracks identified = 9 of 9 (100%).
 - Loss of WT flaws identified = 28 of 35 (80%)
 - Minimum WT loss identified (against total steel plate thickness) = 0.99%.

The ensuing key images (*Figure 5 to Figure 11*) were extrapolated from TomoView® to illustrate the minimum flaw detection characteristics highlighted in Table 4, i.e. L1.5, L1.7.2 and L2.2. The C-scan slices are stacked and oriented into one image to show all detected flaws at their given depths, with palette type and contrast/exposure level also specified.

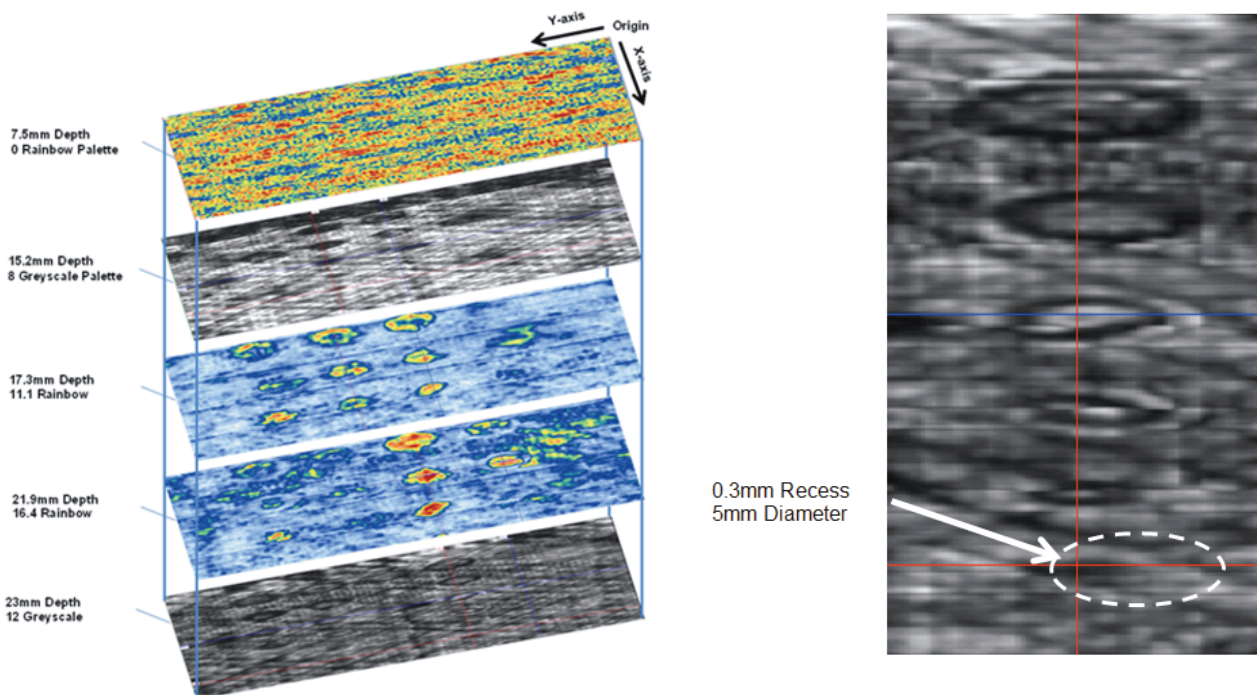


Figure 5 (Left) – L1.5: Test Piece 2 – 5MHz Roller Scanner – 10mm Focal Depth
Figure 6 (Right) – L1.5 Single Plane C-scan at 23mm Depth (Greyscale Palette = 12)

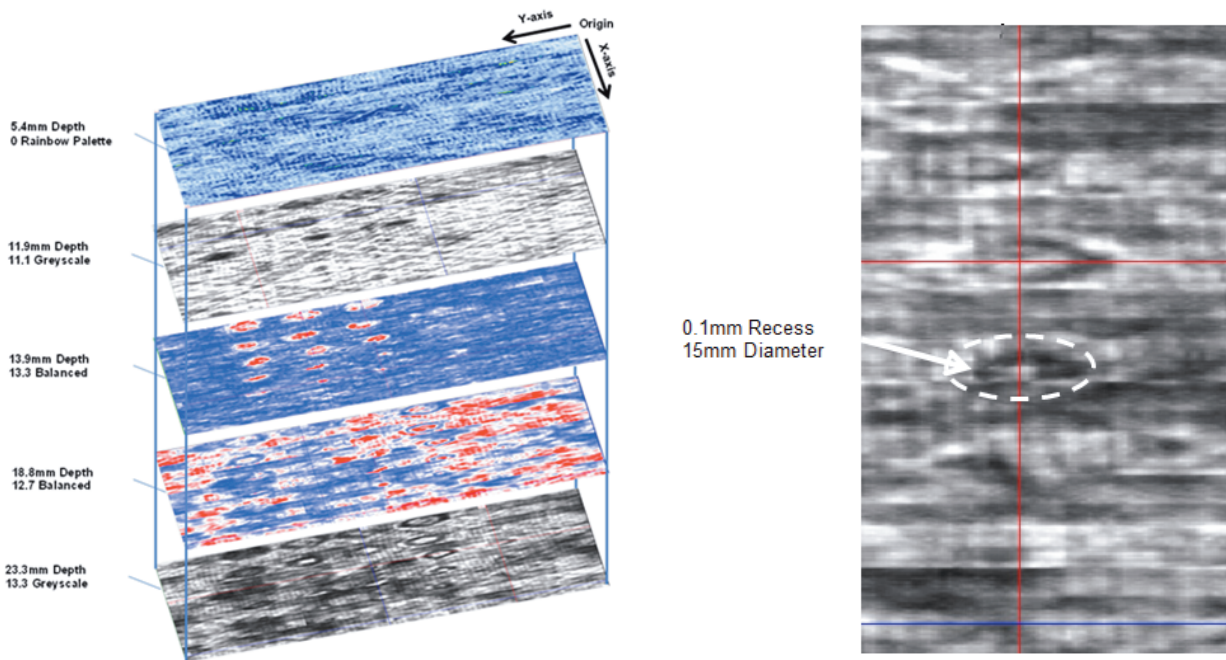


Figure 7 (Left) – L1.7.2: Test Piece 2 – 5MHz (BP 2) Roller Scanner – 15mm FD
Figure 8 (Right) – L1.7.2 Single Plane C-scan at 23.3mm Depth (Greyscale Palette = 13.3)

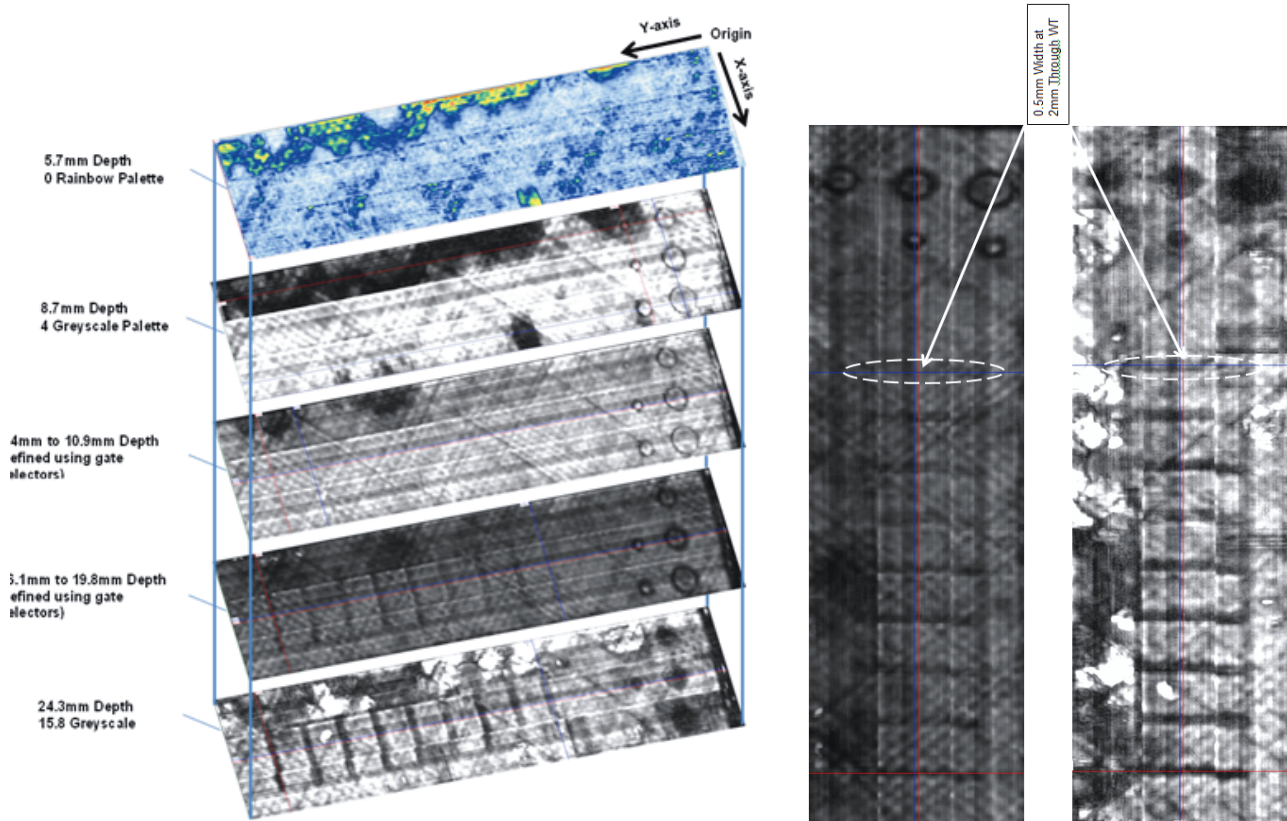


Figure 9 (Left) – L2.2: Test Piece 1 – 5MHz Roller Scanner
Figure 10 (Middle) – L2.2 Single Plane C-scan at 16.1mm to 19.8mm Gate Selector Refined Depth Range
Figure 11 (Right) – L2.2 Single Plane C-scan at 24.3mm Depth Range

© Devonport Royal Dockyard Limited, 2018. Subject to any third party rights, this document and the information contained herein is the unpublished work and property of Devonport Royal Dockyard Limited (DRDL) created in 2018 any copyright in which vests in DRDL. It may not be copied or used for any purpose other than that for which it is supplied without the express prior written consent of DRDL.

3.2.2. GFRP Impact Tests

From an initial visual inspection, Sample-A in Figure 12 shows Barely Visible Impact Damage (BVID) with no signs of de-lamination, whereas samples C and D when held up to the light show significant damage and visual signs of multilayer de-laminations. Samples I and J show surface and back surface rupture and a sign of potential fibre breakout.

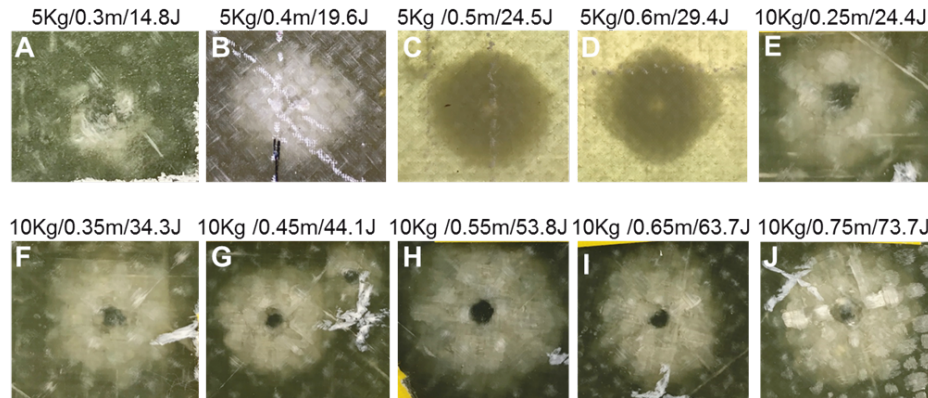


Figure 12 – Impact Test Samples A-J

Sample A, which has the lowest impact energy ($\approx 15J$), had a maximum flaw width of 12mm at the back wall echo and first detection of the flaw at 5mm deep. Sample D (Figure 13) has a relatively medium level of impact energy ($\approx 29J$) and had a maximum flaw width of 67mm and first detection of the flaw at 0.8mm. Sample J has the highest impact energy ($\approx 79J$) and had a maximum flaw width of 60mm and first detection of the flaw at 0.4mm.

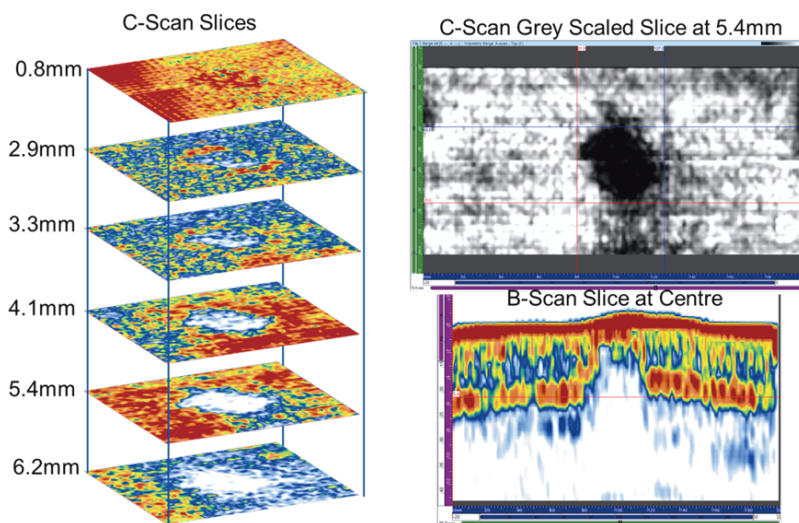


Figure 13 – Sample D (KE $\approx 29J$) Exploded C-scan, B-scan and Grey Scale

All the impacted samples were subjected to optical microscopy with an example of a macro slice (Sample E) shown in Figure 14. Sample E revealed multiple layers of matrix cracking and multiple planar cracks. The planar thin white surface cracks have been identified as non-symmetrical fine de-laminations between two plies. This result was indicative of the majority of samples (B-J).



Figure 14 – Optical Results 6.3x Magnification Impact Sample E - Macro Slice Side on View

3.2.3. GFRP Heat Exposure Tests

The visual results of the heat exposures can be seen in Figure 15.

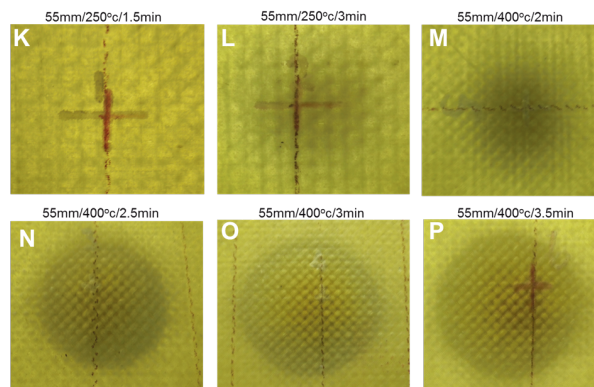


Figure 15 – Heat Exposure Test Samples K-P

Sample O had the largest de-lamination and had 400°C of concentrated heat applied to it at distance of 55mm for 180 seconds. The C-Scan slices, which begin with a negative depth due to the proud blister, can be seen in Figure 16.

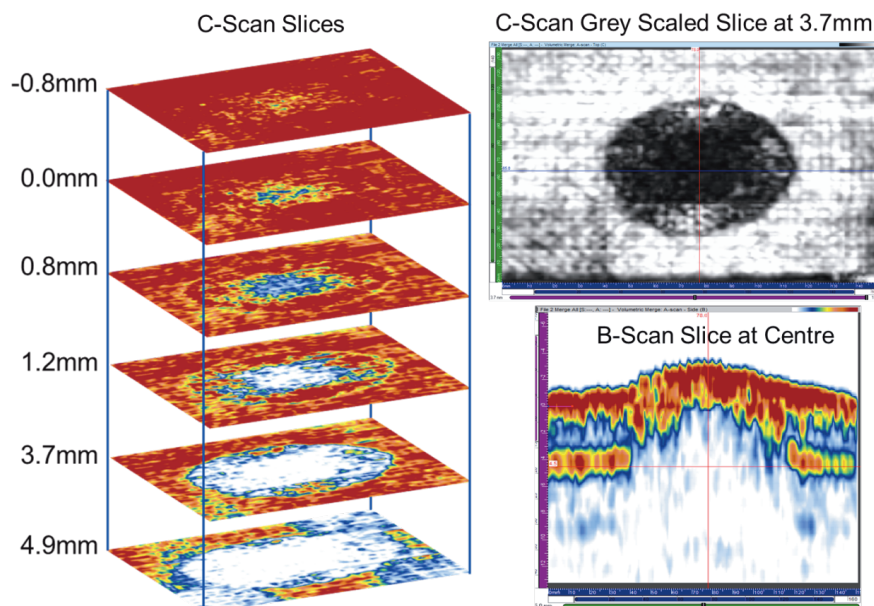


Figure 16 – Sample O (400°C 3min) Exploded C-scan, B-scan and Grey Scale

The samples that were exposed to 400°C for durations of 150 seconds and greater (N, O and P), have symmetrically round surface blisters and surface scorching, which has caused significant subsurface de-laminations. The de-laminations have a width of 62-75mm and a near surface depth of approximately 1.7mm, as shown in Figure 17.

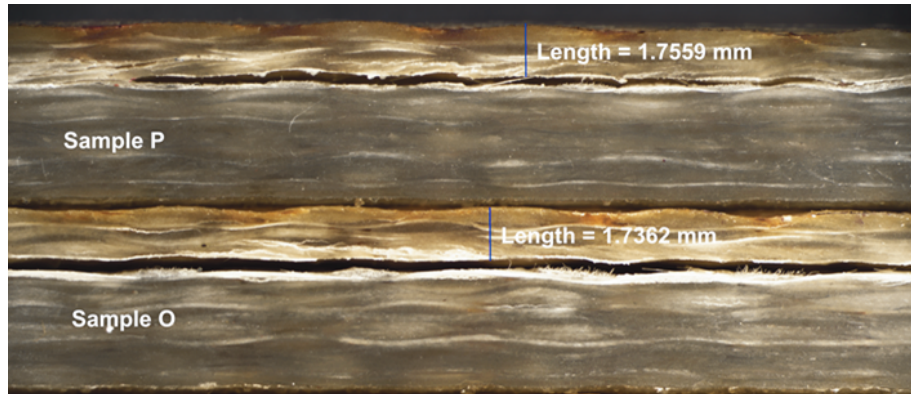


Figure 17 – Heat Exposure Samples - Optical Results – Macro Slice Side on View

There were some artefacts/indications in the optical microscopy results, which could not be qualitatively determined and characterised, and thus were subjected to a scanning electron microscope for further identification. Figure 18 (left Image) shows an area at the edge of a large de-lamination with ambiguity as to what the visual damage is. The SEM (Figure 18 – right image) clarified it as multiple smaller near surface de-laminations as well as fibre breakage.

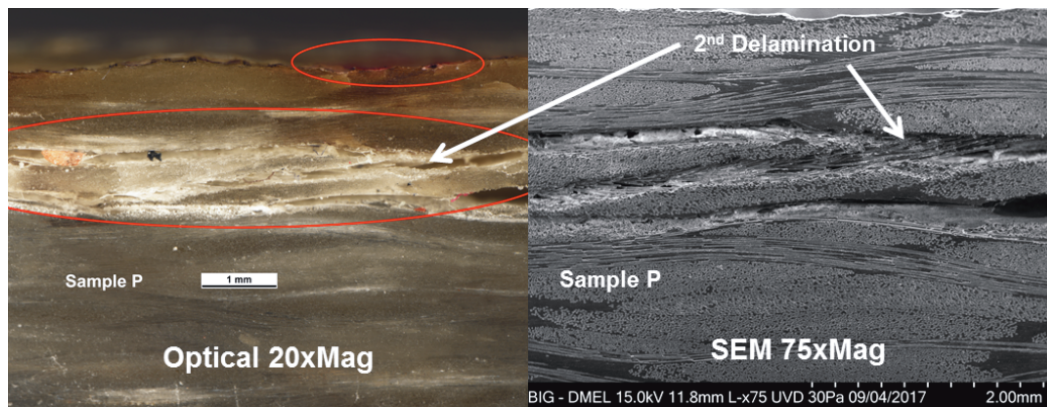


Figure 18 – Sample P - 2nd De-lamination SEM Confirmation

A full list of the identifiable/observable flaws for both the impact and heat exposure test samples, which were verified with microscopy methods (SEM and optical microscope), can be seen in Table 3.

Sample	Destructive Test	Matrix Cracking	Planar Cracks	Fine Delam	Significant Delam	Fibre Breakage	Scorch	Blister
A	Impact 14.76J	✓	✗	✗	✗	✗	✗	✗
B	Impact 19.60J	✓	✓	✓	✗	✗	✗	✗
C	Impact 24.49J	✓	✓	✓	✗	✗	✗	✗
D	Impact 29.41J	✓	✓	✓	✗	✗	✗	✗
E	Impact 24.42J	✓	✓	✓	✗	✗	✗	✗
F	Impact 34.32J	✓	✓	✓	✗	✗	✗	✗
G	Impact 44.10J	✓	✓	✓	✗	✗	✗	✗
H	Impact 53.79J	✓	✓	✓	✗	✗	✗	✗
I	Impact 63.72J	✓	✓	✓	✗	✗	✗	✗
J	Impact 73.73J	✓	✓	✓	✗	✗	✗	✗
K	Heat 250°C-90sec	✗	✗	✗	✗	✗	✗	✗
L	Heat 250°C-180sec	✗	✓	✗	✗	✗	✗	✗
M	Heat 400°C-120sec	✗	✓	✗	✗	✗	✓	✗
N	Heat 400°C-150sec	✗	✓	✗	✓	✓	✓	✓
O	Heat 400°C-180sec	✗	✓	✗	✓	✓	✓	✓
P	Heat 400°C-210sec	✗	✓	✗	✓	✓	✓	✓

Table 3 – Microscopy Table of Results (Impact and Heat Exposure)

© Devonport Royal Dockyard Limited, 2018. Subject to any third party rights, this document and the information contained herein is the unpublished work and property of Devonport Royal Dockyard Limited (DRDL) created in 2018 any copyright in which vests in DRDL. It may not be copied or used for any purpose other than that for which it is supplied without the express prior written consent of DRDL.

3.3. Analysis

3.3.1. CFRP Test Pieces

The laminate produced in the controlled environment, i.e. to promote high V_F and low V_R , improved the scan quality by reducing interference due to attenuation. Although the in-service Test Piece 2 (circles) had reasonable V_F and V_R fractions, the extremely high V_V content of 6.26%, which is a product of poor laminate quality, accentuated the different attenuation properties of the CFRP material when bonded to steel, and as a result any alterations to set-up refinement were unable to identify flaws to an acceptable sensitivity. Hence, low V_V , e.g. <1% is a key factor in the number of identifiable flaws.

The 5MHz probe improved the signal return and therefore was more successful in identifying a larger number of flaws to a higher sensitivity within both laboratory test pieces when compared to the 1MHz probe. The high quality laboratory laminate enabled the 5MHz probe to successfully penetrate the CFRP, and was subsequently more effective as it is the preferred probe frequency for assessing flaws within steel.

Beam steering did not identify any crack flaws within the in-service or laboratory test pieces. A combination of carbon fibre fabric weave, cure inconsistencies, differing material velocity requirements, and differences in CFRP and steel grain structure affected the beam steered angle, which prevented any meaningful data being returned.

PAUT scan accuracy was assessed by correlating scan indication diameters for the loss of wall thickness and de-bonding flaws against their corresponding test piece known diameters. The crack flaw widths were not assessed for accuracy in this way as they could only be similarly measured at ~ 0.75 mm wide due to scan interference. However, the crack lengths within the laboratory scans were all measured at 75mm, in line with their flaw lengths. The laboratory 5MHz scans, representing the scans with the most identified flaws to the highest sensitivity level, had the following sizing accuracy variations:

1. De-bonds:
 - a. 5% for de-bonds ≥ 20 mm diameter.
 - b. 16.7% for de-bonds ≥ 10 mm diameter.
 - c. 60% for de-bonds = 5mm in diameter.
2. Cracks:
 - a. $\sim 0\%$ for lengths ≥ 75 mm (100% accuracy).
 - b. No measured accuracy for widths confirmed as all widths were approximated as 0.75mm.
3. Loss of WT:
 - a. 32.5% for loss of WT ≥ 0.3 mm for diameters ≥ 10 mm.
 - b. 8.5% for loss of WT = 0.1mm for diameters ≥ 15 mm.

The technique allowed detection of 5mm diameter, 0.25mm (single ply) thick PTFE synthetic de-bonds with 100% reliability from all final scan repeats. On average, scans were able to size PTFE de-bonds within 3mm of the known diameter.

The loss of wall thickness analysis capability using PAUT confirmed 0.1mm (0.99%) thickness reductions at 15mm diameter, which could be inspected within 0.75mm (5%) accuracy. This is consistent with baseline steel plate inspection Def-Stan requirements.

3.3.2. GFRP Test Pieces

The damage induced via the drop test shown in the microscopy results is indicative of the 'pyramid-like' stacking sequence that consists of vertical matrix cracking and horizontal planar cracking/de-laminations and is clearly evident in the impact samples. All but one of the impacted samples (Sample A), had both multiple layers of matrix cracking and de-laminations. **Note:** None of the impacted samples appeared to exhibit evidence of fibre breakage or fibre break-out after undergoing microscopy.

The experiment conducted on the heat exposure samples was an accelerated test and is not particularly representative of how blisters are formed. Nonetheless, it was confirmed with the microscopy that a large de-lamination, approximately 1.7mm deep into the laminate, had formed at the centre of each sample. In addition to the large centre delamination, the microscopy confirmed the presence of smaller multilayer de-laminations, cracks

and fibre breakage at the edges of each significant de-lamination. There was also proof of a scorched surface and an obvious proud blister.

There is a distinct difference between the PAUT scan of a significant delamination and a sample that has matrix cracking and fine planar horizontal crack/de-laminations. The horizontal cracks seen in the volumetric slices of the impact Samples A-J are layers of fine one ply irregular shaped de-laminations, as seen in Figure 19 (Left) (p.75-76). If the layers of de-laminations were looked upon in a plan view (C-Scan) they would appear as an outline of all the de-laminations stacked on top of each other, as seen in Figure 19 (Right) (p.75-76). This outline is the unique trace of multi-layered matrix cracking/de-laminations that can be seen in the sliced C-scans from the PAUT scans taken from the samples in this study.

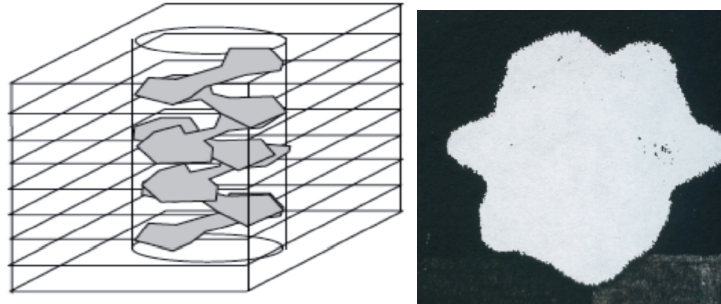


Figure 19 – Layers of Impact De-laminations Formed in Laminate, Morton (p.75-76) © Imperial College London

The samples which were exposed to heat, which subsequently have surface blisters and significantly larger near surface de-laminations, do not give the same PAUT responses as the impacted samples. The geometrical outline of the flaw is a near perfectly symmetrical circular delamination displayed as the absence of sound in the C-Scan and a strong constant curved loss of back wall echo in the B-Scan.

The impacted samples with non-symmetrical C-scan and staggered B-scan outlines is what distinguishes them from the blistered samples, which have symmetrical C-scans with constant curved B-scans; in theory this differentiates them from poor adhesion with high amplitude responses. Individual layered cracks/de-laminations cannot be singled out due to the absence of sound. As soon as one de-lamination occurs, sound will not penetrate any deeper, and hence any de-laminations underneath another one which has occurred near the surface will only appear as an outline which deviates from the shape above it.

3.4. Conclusion

It is the authors' opinion that PAUT is a suitable method for identifying loss of wall thickness (corrosion/pitting) and fatigue cracking perpendicular to the beam in steel when bonded to CFRP, as well de-bonding between the steel to CFRP interface, meeting acceptable assessment criteria in order for a Design Authority to sentence defects adequately. The independent characterisation (morphology) of defects is proven with respect to:

- Blisters resulting in significant de-laminations caused by acute short intervals of high temperature exposure, i.e. a minimum of 400°C for 2.5 minutes.
- Matrix cracking and fine de-lamination/planar cracks identifiable down to a Projectile Kinetic Energy of $\approx 20\text{J}$.
- Matrix cracking/planar cracks caused by impacts, which are distinguished from significant de-laminations caused by blisters due to their unique C-scan and B-scan geometries.

However, in order to successfully introduce either GFRP or CFRP repairs into the industrial environment new lamination methods such as RIFT need to be proven in order to attain the required combination of high fibre volume fractions and low void content to ensure flaw inspection and reliability is not limited by inspection resolution and interference.

The following trends were derived:

- Scanned diameter accuracy is affected by flaw diameter and through thickness, i.e. as diameter decreases average measurement deviation increases, due to scan interference, cure inconsistencies and differences in material grain structure.
- Inversely exponential trend exists between scanned sizing accuracy and resolution.
- Measured flaw dimensions are larger than actual flaw dimensions in ~61% of the test cases, i.e. due to the use of steel velocity.
- Higher laminate V_F and lower V_V reduces interference due to attenuation and results in more accurately sized defects due to improved scan quality.

4. Acknowledgements

The authors would like to thank Mr Gary Whalley, Mr Nick Queen, Mr Robert McHale, Dr Richard Cullen, Babcock International, Newcastle University, Plymouth University and Imperial College London for their input, support, guidance and facilities.

5. References

Smith R, NA, Materials Science and Engineering Volume III – Composite Defects and Their Detection, Available at: <http://www.desware.net/Sample-Chapters/D07/E6-36-04-03.pdf> (Accessed: 10/07/16)

McHale R: “An Investigation into the uses of Advanced Ultrasonic Methods for Detecting Defects in Metal Substrates Bonded to Composite Structures”, DRDL and Newcastle University, United Kingdom, October 2017.

Downing J: “Characterisation of Defects in Composites Utilising a Practical In-Service Ultrasonic Inspection Method”, DRDL and Imperial College, Plymouth/London, United Kingdom, September 2017.

Morton J. *Composites MSc Impact of Composites*. [Lecture] Imperial College London. March 2017.

6. Author’s Biography

James Downing is the NDT Research and Development Manager for Babcock at Devonport Royal Dockyard. He is a Chartered Engineer and Member of IMechE and holds a MSc Degree in Advanced Composite Engineering at the Imperial College of London, and BEng (Hons) Degree in Mechanical Engineering with Composites at the University of Plymouth.

Alex Hook is the Naval Engineering Technology Manager for Babcock Energy and Marine Technology. He is currently completing a MSc in Marine Technology with the Marine Technology Education Consortium through Newcastle University, and has a BSc (Hons) Degree in Marine and Composites Technology with Plymouth University.